Ephaptic coupling of cortical neurons

Article *in* Nature Neuroscience · February 2011

DOI: 10.1038/nn.2727 · Source: PubMed

4 authors:

Costas Anastassiou
Cedars-Sinai Medical Center
64 PUBLICATIONS **9,134** CITATIONS
SEE PROFILE

Rodrigo Perin
École Polytechnique Fédérale de Lausanne
31 PUBLICATIONS **3,389** CITATIONS
SEE PROFILE

Henry Markram
École Polytechnique Fédérale de Lausanne
347 PUBLICATIONS **44,463** CITATIONS
SEE PROFILE

Christof Koch
Allen Institute for Brain Science
984 PUBLICATIONS **123,592** CITATIONS
SEE PROFILE

nature neuroscience

Ephaptic coupling of cortical neurons

Costas A Anastassiou[1,2,5], Rodrigo Perin[3,5], Henry Markram[3] & Christof Koch[1,4]

The electrochemical processes that underlie neural function manifest themselves in ceaseless spatiotemporal field fluctuations. However, extracellular fields feed back onto the electric potential across the neuronal membrane via ephaptic coupling, independent of synapses. The extent to which such ephaptic coupling alters the functioning of neurons under physiological conditions remains unclear. To address this question, we stimulated and recorded from rat cortical pyramidal neurons in slices with a 12-electrode setup. We found that extracellular fields induced ephaptically mediated changes in the somatic membrane potential that were less than 0.5 mV under subthreshold conditions. Despite their small size, these fields could strongly entrain action potentials, particularly for slow (<8 Hz) fluctuations of the extracellular field. Finally, we simultaneously measured from up to four patched neurons located proximally to each other. Our findings indicate that endogenous brain activity can causally affect neural function through field effects under physiological conditions.

Neurons communicate via specialized molecular machines, the synapses. Such discrete, point-to-point synaptic connectivity, whether chemical or electric, is important for information processing in the brain[1–3]. However, such integrative processes do not occur in a vacuum. Instead, neurons are located in a conductive medium, the extracellular space. Synaptic inputs, their integration and spike generation trigger changes in the electric potential V_e outside the cell that decay with distance from the current source. The measured V_e are the superimposed V_e contributions from all cellular processes at any given point. The local field potential (LFP) is the low-pass component (typically below 300 Hz) of V_e. Although the extracellular signature of individual neurons, such as extracellular action potentials, has a modest and spatially confined amplitude[4,5], coordinated synaptic input in a specific brain region, for example, cortical slow waves[6,7], hippocampal theta[8–11] or sharp waves/ripples[12,13], gives rise to more prominent spatiotemporal LFP oscillations. Their distant echoes can be picked up outside the skull by EEG electrodes. As V_e differs from location to location, an electric field E (the negative spatial gradient of V_e) arises. Such fields, in turn, cause changes in the membrane potential V_m through ephaptic coupling[14–20] (the term 'ephapse' was coined[14] to describe electric field interactions occurring between juxtaposed neural elements; we use it to describe effects induced by voltage and field changes along the cell membrane in general[17]). In other words, groups of cells change their local electric environment, which in turn feeds back onto the electric activity of all of its members. These ephaptic effects occur in addition to any direct synaptic coupling among cells. Although ephaptically induced changes in V_m under physiological conditions cannot give rise to action potentials when V_m is around rest[16,20], ephaptic events may affect the spike timing of individual neurons receiving suprathreshold synaptic input[16,18,21,22], as well as neural populations firing under pathological conditions[19,23–25]. Moreover, extracranial application of slowly varying currents can affect behavior, enhancing, for example, sleep-assisted memory consolidation in humans[26]. Robust relationships between the oscillating LFP and spiking are widely observed[27–32]. However, these have been solely attributed to direct synaptic interactions. We examined the extent to which ephaptic coupling to LFP-like fluctuations alters the subthreshold and suprathreshold response of neurons. We found that changes in the electric field, as typically measured during *in vivo* LFP activity, substantially altered the electric response of rodent cortical pyramidal neurons.

Endogenous electric field activity in the living brain typically induces extracellular voltage changes less than 0.5 mV and fields under 5 mV mm^{-1} (refs. 12,33,34). Whether this is sufficient to modulate activity of individual neurons has not been easy to address because of the difficulty of teasing apart synaptic effects from ephaptic ones. Most studies have focused on network interactions by applying constant fields along parallel plates outside the slice preparation even though such extracellular fields lack *in vivo*–like spatial features[35]. Furthermore, only a single extracellular electrode has been used to monitor V_e at least 50 µm away from the soma, making estimation of the real V_e and the induced E at the somatic membrane problematic. Although these pioneering experiments were critical in demonstrating that constant fields of modest amplitude extending across millimeters may affect neural activity, they could not, and do not, address ephaptic coupling at the single-compartment (somatic membrane) level. This, however, is necessary for a proper mechanistic understanding of the influence of the LFP on single cells during cognitive tasks in both animals[27–29,36–38] and humans[32,39,40].

RESULTS

Electric stimulation inside and outside of individual neurons while concurrently monitoring the induced extracellular field at specific locations (for example, just outside the soma) requires multiple pipettes in a confined space. We developed a 12-pipette setup that

[1]Division of Biology, California Institute of Technology, Pasadena, California, USA. [2]Department of Bioengineering, Imperial College, London, UK. [3]Laboratory of Neural Microcircuitry, EPFL, Lausanne, Switzerland. [4]Department of Brain and Cognitive Engineering, Korea University, Seoul, South Korea. [5]These authors contributed equally to the work. Correspondence should be addressed to C.A.A. (costas@caltech.edu).

Received 6 October 2010; accepted 30 November 2010; published online 16 January 2011; doi:10.1038/nn.2727

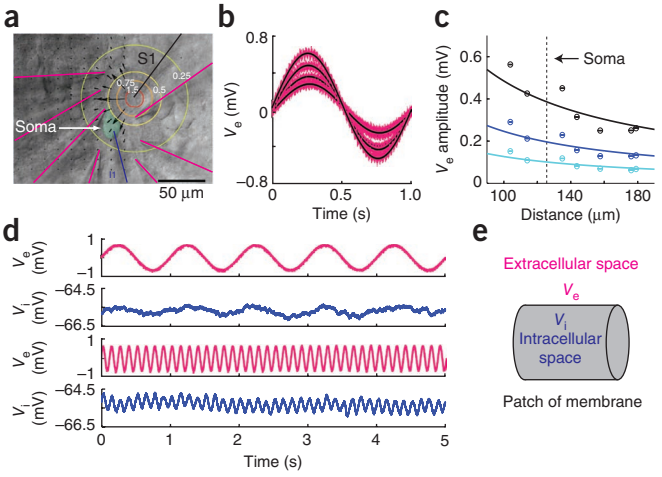

Figure 1 Simultaneous recordings from up to 12 electrodes inside and outside a single neuron in rat slice during intra- and extracellular stimulation. (**a**) Unipolar stimulation (I_0 = 200 nA at 1 Hz) in slice via an extracellular pipette (S1) near the soma of a patched pyramidal neuron (intracellular pipette, I1). (**b**) Seven extracellular pipettes were positioned close to the soma of the patched neuron to monitor V_e (magenta, V_e recordings; black, mean waveform after 9-s stimulation). The isopotentials are shown in **a** (blue, sink; red, source). (**c**) V_e amplitude as a function of pipette location for I_0 = 50 (cyan), 100 (blue) and 200 (black) nA (circles, mean; error bars, s.d.). Distance is calculated from the tip of the extracellular stimulating electrode S1. Solid lines indicate the point-source approximation (least-squares fitting; typically the extracellular resistivity ρ = 2.5–3.8 Ωm, ref. 41). (**d**) Perturbing V_e (magenta) through extracellular stimulation from pipette S1 caused V_i to change (blue) through ephaptic coupling (top traces, I_0 = 100 nA and f = 1 Hz; bottom traces, I_0 = 100 nA and f = 8 Hz). (**e**) The membrane potential V_m was defined as $V_m = V_i - V_e$.

allows independent positioning of each pipette under visual control with micrometer accuracy, with the flexibility of using an arbitrary number of these as patching, extracellularly stimulating or extracellular recording pipettes. We stimulated layer 5 neocortical pyramidal neurons in slices while recording inside and outside of their cell bodies. Typically, a single extracellular stimulation electrode (S1) was positioned 50–150 µm from the cell body (**Fig. 1a**). The soma was whole-cell patch-clamped with one intracellular electrode and was surrounded by a number of extracellular pipettes monitoring V_e. The induced electric field as a function of distance from S1 was estimated through the spatial gradient of the best fit of all V_e traces (least-squares fitting; **Fig. 1b**,**c** and **Supplementary Fig. 1**) assuming a point-source approximation[41]. V_e was taken to be the potential at the extracellular recording site closest to the cell body, typically within 15 µm. The relevant V_m was determined by subtracting V_e from V_i (**Fig. 1d**,**e**). Synaptic activity was always pharmacologically silenced using D(−)-2-amino-5-phosphonovaleric acid (AP5) to block NMDA receptors, gabazine or bicuculline to block GABA receptors, and 6-cyano-7-nitroquinoxaline-2,3-dione (CNQX) to block AMPA receptors (see Online Methods and ref. 19). Gap junctions are unlikely to contribute in any substantial manner to our results, as they are both rare among layer 5 neurons at postnatal day 14 (ref. 42), the minimum developmental age of our animals, and leave a telltale sign of spikelets, which we looked for but failed to find (**Supplementary Fig. 2**). Thus, any observed changes in V_m can be solely attributed to the effect of the field, rather than to synapses. Finally, the extracellular stimuli that we applied were always (at least) 25–50-fold weaker than the lowest reported stimulation amplitude (5–10 µA) required to directly trigger action potentials in cortical neurons from rest[43].

We first injected an oscillatory current I of variable strength I_0 and frequency f, with $I = I_0 \sin(2\pi ft)$, through the extracellular stimulation electrode S1 while V_e and V_i were monitored and V_m was calculated by subtracting V_e from V_i, that is, $V_m = V_i - V_e$ (5-s duration, 1–2 repetitions in 23 cells; **Figs. 1a–c** and **2a**). In a perfectly homogenous resistive milieu, a point source induces a V_e that oscillates at the same frequency f, and decays with $1/r$ where r is the distance between S1 and the measurement point[41]. It also induces an E that oscillates at f and decays with $1/r^2$. Notably, *in vivo* extracellular activity does not give rise to distinctive frequency bandwidths but instead scales as $1/f^n$, where the exponent n is approximately 1, over the whole frequency domain[44]. Still, linearly decomposing LFPs into their individual sinusoidal components per the Fourier theorem, although an approximation, is very widespread and not unreasonable. We chose I_0 to induce field and voltage profiles similar to LFPs measured *in vivo*. For extracellular stimulation at 1 Hz with I_0 = 25, 50, 100 and 200 nA, we measured fields of 0.74 ± 0.53, 1.49 ± 1.06, 2.96 ± 2.11 and 5.86 ± 4.25 mV mm^{-1} and V_e amplitudes of 0.07 ± 0.04, 0.14 ± 0.08, 0.28 ± 0.16 and 0.55 ± 0.32 mV, respectively (mean ± s.d.; see also **Supplementary Fig. 1**).

What are the characteristics of V_m entrainment to these spatiotemporal E and V_e fluctuations? We first quantified ephaptic coupling when V_m remained subthreshold (that is, nonspiking). Frequencies of 1, 8, 30, 60 and 100 Hz, emulating the LFP frequencies that cover delta, theta, beta and gamma bands, did not substantially alter the induced E and V_e characteristics (**Fig. 2b**,**c** and **Supplementary Fig. 2**)[41]. Subthreshold oscillations in the membrane potential induced by the extracellular oscillating field through ephaptic coupling persist with equal strength up to 100 Hz (I_0 = 100 nA; for f = 1 Hz, V_m amplitude of 0.16 ± 0.005 mV with a phase of 165° ± 1° between V_m and V_e; for f = 100 Hz, V_m amplitude of 0.14 ± 0.007 mV and a phase of 179° ± 3°; mean ± standard error mean; **Fig. 2b**,**d**). As expected, this led to an anti-phase relationship between V_e (and V_i) and V_m (ref. 45), as determined by the mean properties (**Fig. 2b**) and cross-correlation analysis (**Fig. 2d**). These results are in contrast with those of parallel-plate experiments, which found a strong attenuation of subthreshold V_m amplitudes with increasing extracellular stimulus frequencies[19]. We attribute this disparity to the limited access previous experimental studies have had to the space immediately outside the soma because of the parallel plate geometry and sampling of the field by a single electrode. This made assessing the entrainment of the membrane to the field problematic, in particular given the presence of local tissue inhomogeneities[19]. Notably, ephaptic coupling persists for high-frequency stimuli in contrast with direct intracellular (subthreshold) current injections (**Fig. 2b**), whose effects on V_i are substantially attenuated as a result of capacitive filtering[1].

We tested whether the characteristics of ephaptic coupling persist for different levels of membrane polarization by directly injecting subthreshold currents (I_{inj}) into the cell (**Fig. 2a**). We found that the anti-phase relationship between V_e (and V_i) and V_m remains (**Fig. 2c**,**e**) for all membrane polarization levels (f = 8 Hz and I_0 = 100 nA; for I_{inj} = −150 pA, the induced ephaptic amplitude was 0.13 ± 0.01 mV at a phase of 170° ± 4°; for I_{inj} = 100 pA, the V_m amplitude was 0.13 ± 0.01 mV at a phase of 151° ± 5°; mean ± s.e.m.; **Fig. 2c**,**e**). We conclude that LFP-like extracellular field activity readily entrains the subthreshold membrane potential over a hundred-fold range in frequency and at all tested membrane polarization levels.

We next examined the effect of ephaptic coupling on spiking in 25 cells. We injected a constant current for 9 s at the cell body that

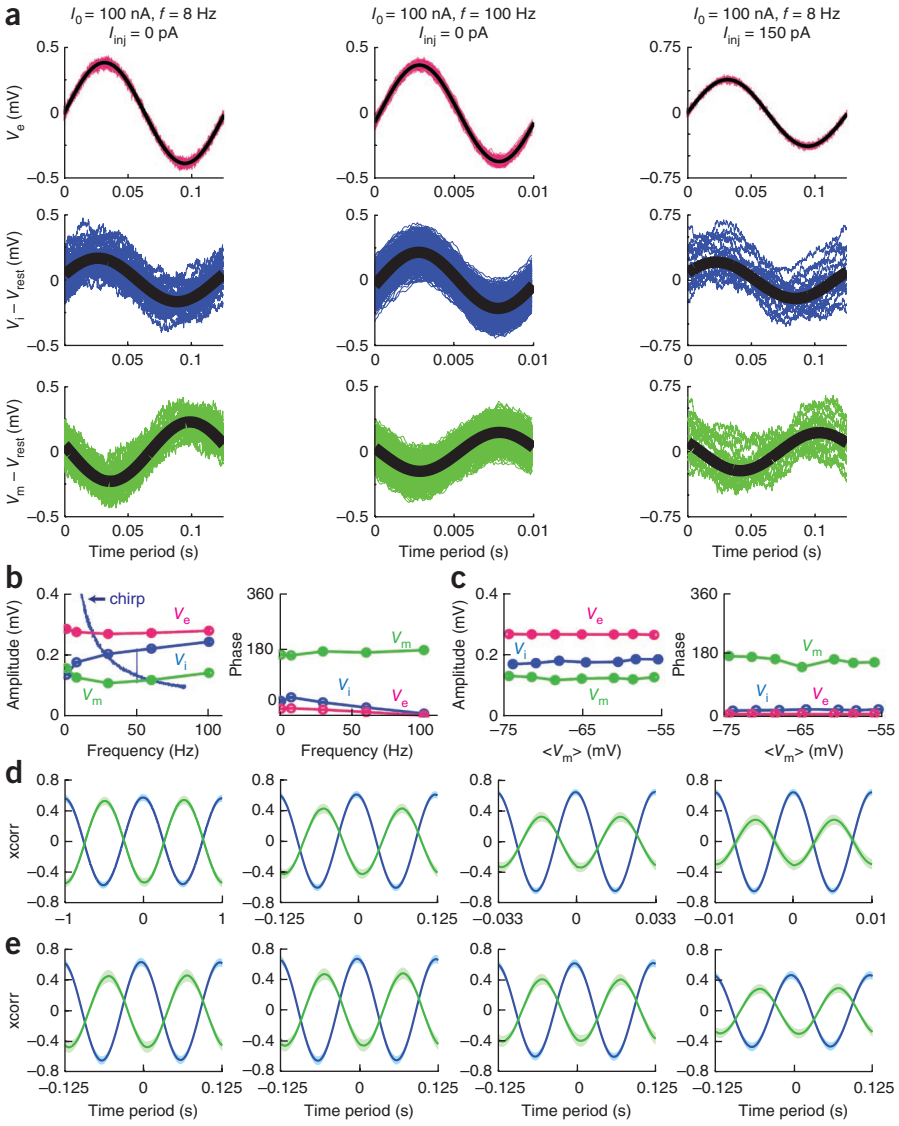

Figure 2 Subthreshold extracellular field entrainment. (**a**) V_e (first row in magenta, mean in black), V_i (second row in blue) and V_m (third row in green) for one neuron for three stimulation regimes: slow and fast extracellular stimulation without intracellular depolarization (left and middle, respectively), and slow extracellular stimulation combined with sustained intracellular current injection (right). (**b**) Amplitude and phase (circles, mean; error bars, s.e.m.) of the V_e (magenta), V_i (blue) and V_m deflection (green) for extracellular stimulation frequencies of 1–100 Hz and constant I_0 = 100 nA (n = 23 cells). V_i attenuation of an intracellular chirp without any extracellular field (blue line; chirp amplitude, 75 pA; frequency $f = 3t$ where t (s) is time). (**c**) Amplitude and phase of the V_e (magenta), V_i (blue) and V_m deflection (green) as a function of membrane polarization (n = 17 cells; circles, mean; error bars, s.e.m.; stimulation frequency f = 8 Hz). (**d**) Normalized cross correlation (xcorr) between V_i and V_e (blue) as well as V_m and V_e (green) of the data shown in **b** (line, mean; shadowed area, s.e.m.) for (left to right) f = 1, 8, 30 and 100 Hz. The difference between xcorr(V_i, V_e) and xcorr(V_m, V_e) for each frequency at one, two and three quarters of the inverse of the stimulation frequency was always highly significant ($P < 0.001$; paired t test Bonferroni-corrected for multiple comparisons). (**e**) xcorr(V_i, V_e; blue) and xcorr(V_m, V_e; green) for the data in **c** (line, mean; shadowed area, s.e.m.) for (left to right) I_{inj} = –150, 0, 50 and 100 pA at f = 8 Hz.

induced spiking (typically 2–4 Hz; **Fig. 3a** and **Supplementary Fig. 3**). Experiments were divided into two groups: control, in which the intracellular stimulus was given without any extracellular field, and extracellular stimulation, in which both intracellular and extracellular stimuli were simultaneously applied (**Fig. 3a–c**). We performed the control experiment immediately before each extracellular stimulation experiment using the same intracellular current step. Each pair (control, extracellular stimulation) was repeated 4–6 times for each field configuration at 1, 8 and 30 Hz.

Although the imposed external field did not substantially change the number of spikes triggered by the current step (**Supplementary Fig. 3**), it did shift their timing. We employed a population-vector analysis (**Fig. 3d** and **Supplementary Figs. 4–9**) to examine whether spikes were elicited at a preferred phase of V_e. We used the Rayleigh criterion to test whether the phase of spikes, relative to V_e, were distributed nonuniformly in the circular phase space (0°, 360°). Indeed, increasing field strength led to an increased deformation of the spike-phase distribution. The increased entrainment manifested itself in the length of the population vector. At a stimulation frequency of 1 Hz and amplitude of 25, 50, 100 or 200 nA, the normalized length of the population vector was 0.046, 0.060, 0.098 and 0.145, respectively, and its direction was 266°, 250°, 242° and 241°, respectively. Note that the preferred spike phase for f = 1 Hz was very similar to the phase of the V_m peak in the subthreshold experiments (**Fig. 2a–c**).

As a further measure of entrainment, we quantified the spike-triggered average (STA) of all neurons (**Fig. 3c**). We calculated the power spectrum of the STA as a function of frequency (**Fig. 3e** and **Supplementary Figs. 4–9**). Increasing the field enhanced the phase locking of spikes to the applied field. To confirm whether this increase is solely attributable to the presence of the field, we assumed a (virtual) V_e identical to the subsequent applied extracellular field so that phases could be ascribed to the spike times of control experiments. The increase in the mean STA spectrum at f with the field (extracellular stimulation) was always greater than without it (control) (**Fig. 3e**).

Cross-correlation and STA depend not only on the degree of phase locking of spikes to the field but also on the amplitude of V_e. We used spike field coherence (SFC), a modified version of the STA analysis[28,32], to quantify the relationship between spiking and the extracellular stimulus. The SFC is defined as the STA spectrum normalized by the power spectra of all V_e segments that were averaged to obtain the STA[28]. The latter is defined as the spike-triggered power (STP). SFC ranges between 0 and 100%, with 0% indicating no phase relationship between spikes and the imposed field and 100% indicating complete phase locking of all spikes to one particular phase. SFC is an accurate indicator of the magnitude of stereotypy of spike time relative to V_e fluctuations[28]. Given that ephaptic coupling increased the STA spectrum at f (**Fig. 3e** and **Supplementary Figs. 4**, **6** and **8**), we compared the SFC between control and experiments at f for each field

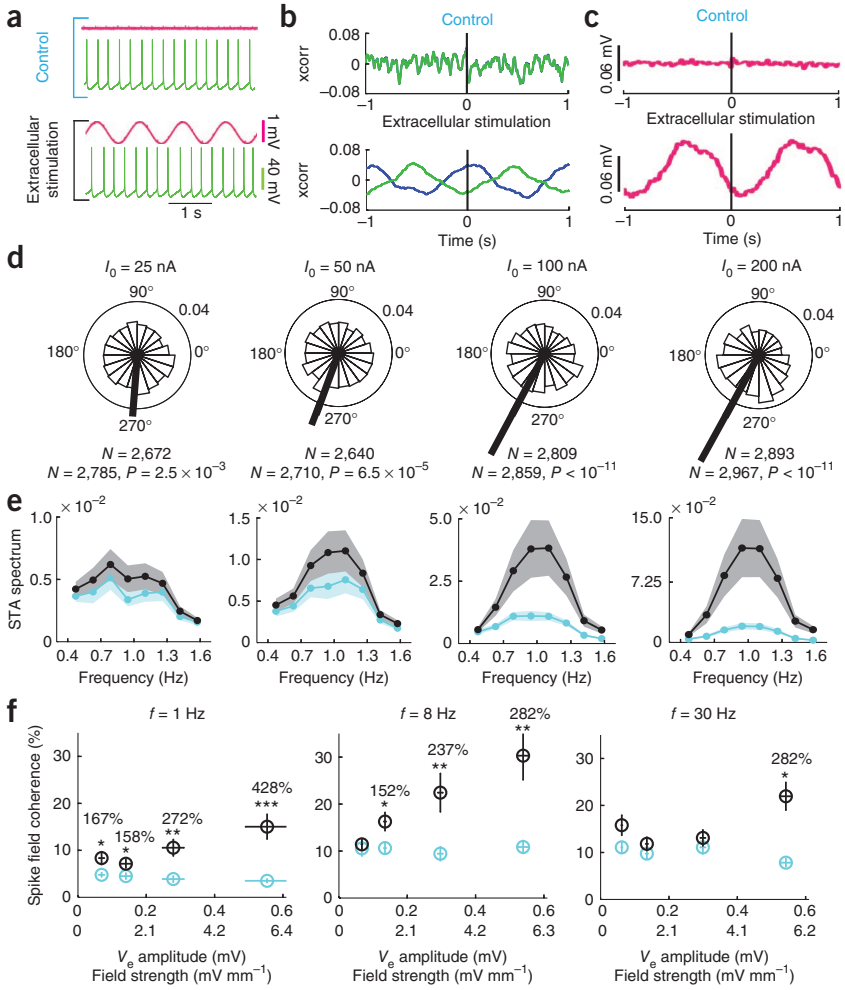

Figure 3 Weak electric fields entrain spiking activity of individual neurons. (**a**) V_e (magenta) and V_m (green) without (control) and with an extracellular field (f = 1 Hz). (**b**) Normalized cross-correlation (xcorr) between V_i and V_e (blue) and V_m and V_e (green) of the low-pass (<100 Hz) suprathreshold data of an individual neuron without (top) and with extracellular stimulation (bottom) at f = 1 Hz and I_0 = 200 nA. (**c**) STA spectra (same data as in **b**; top, control; bottom, extracellular stimulation). (**d**) Population vector analyses for f = 1 Hz (left to right, I_0 = 25, 50, 100 and 200 nA; n = 25 neurons). Field entrainment of spikes led to nonuniform spike-phase distribution (P values by Rayleigh test) that was not attributable to changes in spike number (N(upper), control; N(lower), extracellular stimulation; **Supplementary Fig. 3**). (**e**) STA spectra (circles, mean; shadowed areas, s.e.m.) for the data in **d**. For the control experiments, a (virtual) V_e identical to the subsequent extracellular stimulation experiment was assumed. (**f**) SFC (circles, mean; error bars, s.e.m.) for extracellular stimulation (black) and control (cyan) experiments at (left to right) 1, 8 and 30 Hz as a function of stimulation strength (x axis: first row, circles indicate mean V_e amplitude at the soma and error bars indicate s.e.m.; second row, circles indicate mean E amplitude at the soma). Asterisks indicate statistical significance of the SFC difference between control and extracellular stimulation (paired t test, fdr-corrected for multiple comparisons; *P < 0.05, **P < 0.01, ***P < 0.001). The percentage increase in SFC relative to control is shown for statistically significant changes. STP, STA and SFC are shown for four individual neurons for all stimulation amplitudes and frequencies in **Supplementary Figures 5**, **7** and **9**.

configuration (**Fig. 3f** and **Supplementary Figs. 4**, **6** and **8**). Indeed, the external field clearly increased the SFC by ephaptic coupling. Notably, the significance of the entrainment, as assayed through a paired t test (false discovery rate (fdr)-corrected for multiple comparisons), decreased for increasing stimulus frequency (I_0 = 50 nA; f = 1 Hz, $P = 6.5 \times 10^{-5}$; f = 8 Hz, P = 0.019; f = 30 Hz, P > 0.05). Thus, although an external field as small as 0.74 mV mm^{-1} (V_e amplitude of 0.07 mV) led to statistically significant entrainment at 1 Hz ($P = 6.5 \times 10^{-5}$), the field had to be almost an order of magnitude larger (5.58 mV mm^{-1}, with V_e amplitude of 0.54 mV) for entrainment at 30 Hz to become significant. Ephaptically induced phase locking of spiking is thus more effective, and occurs at lower field strengths, for slow rather than fast modulations of E and V_e.

The enhanced phase locking of spikes to the external field was not a result of changes in the firing rate. This was confirmed by paired t test (Bonferroni corrected for multiple comparison) that showed no statistically significant change (at q = 0.05) in the number of spikes or the spike frequency between stimulation and control experiments (**Fig. 3d** and **Supplementary Fig. 3**). The same null result was also obtained when computing the STP for stimulation and control procedures (**Supplementary Figs. 4**, **6** and **8**). The STP quantifies the oscillations that are present in the V_e signal regardless of whether or not they are related to the occurrence of spikes and is calculated by averaging the power spectrum of each individual V_e segment centered on each spike[28]. Although the average STP of all neurons indicated the strong presence of oscillations (**Supplementary Figs. 4**–**9**), the power of the STP at f did not distinguish between extracellular stimulation and control experiments (paired t test; for all stimulation frequencies, all comparisons between the STP of control and extracellular stimulation experiments resulted in P > 0.58). Thus, the increase in phase locking is attributed to ephaptic entrainment of spikes rather than to a change in firing rate or variations in the STP.

Our results indicate that LFP-like fluctuations in the extracellular potential, V_e, readily entrain both the subthreshold membrane potential and spike trains. Because the LFP extends over hundreds of micrometers, these fields could serve to synchronize thousands of neurons that would otherwise operate independently. To directly test for this, we simultaneously patched four neurons and positioned the extracellular stimulation electrode S1 close by so that all four experienced a simultaneous and similar V_e fluctuation at their cell bodies. Seven extracellular recording electrodes monitored V_e close to the somata of the four neurons and the space between them (**Fig. 4a**). We simultaneously injected a suprathreshold current step (duration of 9 s) into all four cells with or without an external field (**Fig. 4b**). Although the extent to which the membrane potential of each cell was modulated by the field varied (mainly as a result of the varying distance from S1), spike trains in all cells were entrained by the extracellular field, as assessed by the deviation of spike phases from uniformity. Consistent with the single-neuron data, a field oscillating at 1 Hz synchronized spikes in all four cells such that a

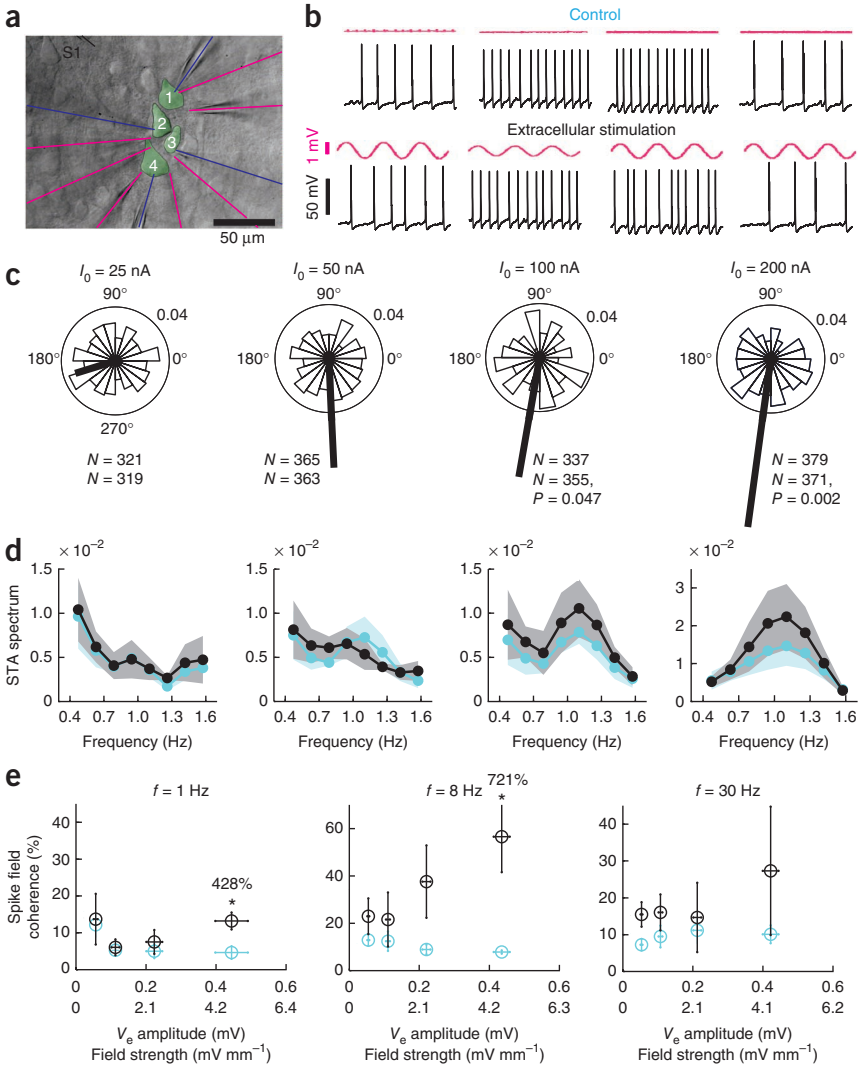

Figure 4 Ephaptic coupling leads to coordinated spiking activity among nearby neurons. (**a**) Four neurons with somata located within 100 µm of tissue were patched with intracellular electrodes (blue). Seven extracellular electrodes monitored V_e fluctuations (magenta). The extracellular stimulation electrode (S1) was 50–80 µm from the four somata. (**b**) Intracellular (black) and extracellular (magenta) activity during concurrent intracellular current injection to the four neurons (top, control; bottom, extracellular stimulation with I_0 = 100 nA and f = 1 Hz). (**c**) Population vector analysis of all spikes from neurons 1–4 for (left to right) I_0 = 25, 50, 100 and 200 nA and f = 1 Hz. As field strength increased, spikes from all neurons clustered around 270° (left to right, mean population vector angle, 197°, 272°, 260°, 262°) and the phase distribution significantly deviated from uniformity (P values by the Rayleigh test). There was no significant change in firing rate ($P > 0.1$) (N(upper), control; N(lower), extracellular stimulation). (**d**) STA spectra (circles, mean; shadowed areas, s.e.m.) for the data in **c** (cyan, control; black, extracellular stimulation). (**e**) SFC (circles, mean; error bars, s.e.m.) for extracellular stimulation (black) and control (cyan) experiments at (left to right) 1, 8 and 30 Hz as a function of stimulation strength (x axis: first row, circles indicate mean V_e amplitude at the soma, error bars indicate s.e.m.; second row, circles indicate mean E amplitude at the soma). Asterisks indicate a significant difference in SFC between control and extracellular stimulation experiments (paired t test, fdr-corrected for multiple comparisons; $^*P < 0.05$). The percentage increase in SFC relative to control is shown for statistically significant changes. STP, STA and SFC for each neuron individually are shown in **Supplementary Figures 11–13**.

preferred spiking-phase close to 270° emerged with increasing field strength (**Fig. 4c–e**). Note that all of this took place without any synaptic transmission occurring (**Supplementary Fig. 10**), as a result of the synaptic blockers that we used. This phase preference cannot be attributed to differences in firing rates between the two conditions (**Supplementary Figs. 11–13**). We observed the same outcome when simultaneously patching triplets (**Supplementary Fig. 14**) and pairs (**Supplementary Fig. 15**) of neurons.

DISCUSSION

The subthreshold V_i oscillations that we found that are in lock-step with the imposed V_e oscillations in the extracellular field bear the hallmarks of ephaptic potentials. These were changes in the membrane potential V_m along an extended neuronal cable caused by an external electric field and are a simple consequence of Kirchhoffs' circuit laws. Their amplitude was below 0.5 mV, consistent with theoretical estimates[20]. These potentials remained undiminished at frequencies up to 100 Hz and were independent of synaptic input, as all receptors were pharmacologically blocked. Given the small amplitude of ephaptic potentials relative to the spiking threshold that is approximately 25 mV above rest, it is not clear how they could have any substantial role in the life of a spiking neuron. To evaluate whether they can, we induced pyramidal neurons to fire action potentials at 2–4 Hz (**Supplementary Fig. 3**) by direct current injection. Indeed, the modest (in amplitude) electric field did not trigger any additional action potentials. However, it did induce substantial shifts in the timing of these action potentials. Even very small and slowly changing fields that triggered V_e changes under 0.2 mV led to phase locking of spikes to the external field and to a greatly enhanced spike-field synchrony. This high sensitivity of spike timing to small, but persistent, oscillations that act throughout a volume needs to be contrasted with the intrinsic, that is, nonsynaptic, noise in layer 5 pyramidal neurons of 0.2–0.4 mV[46] and to the much larger noise if synaptic background activity is taken into account. Notably, the magnitude of the minimal electric fields causally effective (approximately 1 mV mm^{-1}) is comparable to the intracranial fields applied by electrodes outside the skull in human studies[26]. The oscillations causing the greatest effect (1 Hz) mimicked the frequency of cortical slow waves, a common rhythm observed during natural sleep and under anesthesia[6,7,26]. Although these effects persisted for frequencies up to 8 Hz, that is, the theta bandwidth, they became gradually smaller as the field frequency increases. At 30 Hz, only the largest external field still had an effect, almost tripling the SFC.

What mechanism could be responsible for the entrainment of spikes to modest (in strength) and slow (in temporal frequency) extracellular field oscillations? One explanation could involve the

resonant properties of neurons. Individual neurons can have frequency preferences that enable them to respond best to inputs in a narrow frequency window[47]. In the presence of a suprathreshold intracellular direct current input, V_e oscillations might induce such frequency-specific spiking. However, when examining the V_m response induced by the suprathreshold dc input without an extracellular field (control experiments), the resulting V_m fluctuations were substantial and their amplitude greatly exceeds that induced through ephaptic coupling (**Supplementary Fig. 16**). Thus, membrane resonance to weak oscillatory extracellular stimuli seems to be an implausible mechanism given the strong intracellular fluctuations induced by direct intracellular dc injection.

An alternative explanation is that, for slow stimuli, the neural membrane can be described by a simple phenomenological model with constant firing threshold[18,20]. If it takes synaptic input 100 ms to reach a 10-mV spike threshold, then a 0.5-mV ephaptic potential will phase advance the next spike by 5 ms (**Supplementary Discussion** and **Supplementary Fig. 17**). An oscillatory extracellular field along a neuron receiving strong intracellular input leads to periodic polarization of the membrane and the emergence of spike-phase preferences[20]. For faster extracellular stimuli, a possible combination of various spiking-associated currents and differential entrainment of the different neural compartments leads to the gradual loss of such spike-phase preference[20].

Our results suggest that periodic membrane polarization resulting from ephaptic coupling to the slow frequencies of the LFP define temporal windows of enhanced excitability across the cells experiencing this field[20,30,31]. Such phase coding with reference to the slow (1–8 Hz) ongoing LFP signal has been shown to provide substantial enhancement of mutual information in coexistence with other codes, such as spatial and temporal spike patterns, as well as increased robustness[27,36,48,49]. Using a setup that allowed us to control and measure electric fields and potentials at up to 12 locations inside and outside an individual neuron at high fidelity, we examined the manner in which an external field leads to phase locking of individual neurons, as well as spike synchrony among quartets, triplets and pairs of nearby neurons.

How relevant is ephaptic coupling, obtained here under artificial (slice) conditions, to the living brain? The amplitudes of our extracellular potentials (up to 0.6 mV) and fields (up to 6 mV mm^{-1}) were comparable to the amplitudes of LFPs measured under natural conditions. Furthermore, our changes in SFC were as large, or larger, than those observed in cortex. For instance, successful memory formation in humans is predicted by a tight coordination of spike timing in hippocampal neurons to the local theta oscillation, with SFC increase of approximately 50% compared to unsuccessful trials[32]. These changes are entirely consistent with our measured ephaptic coupling to the LFP and were associated with V_e and E amplitudes of 0.1 mV and 1 mV mm^{-1} (**Fig. 3f**). Finally, the fields induced in our experiments were comparable to fields applied outside the skull that have been shown to alter cognitive processes in humans[26].

Our results support the notion that ephaptic potentials induced by oscillating electric fields present throughout the gray matter serve to synchronize neuronal activity with little regard to whether excitatory or inhibitory. Such synchronization may have a substantial effect on neural information processing and plasticity.

METHODS

Methods and any associated references are available in the online version of the paper at http://www.nature.com/natureneuroscience/.

Note: Supplementary information is available on the Nature Neuroscience website.

ACKNOWLEDGMENTS

We thank G. Buzsáki, U. Rutishauser and E. Schomburg for comments and discussions and J. Bastiaansen for assistance. This work was funded by the Engineering Physical Sciences Research Council (C.A.A.), the Sloan-Swartz Foundation (C.A.A.), the Swiss National Science Foundation (C.A.A.), EU Synapse (R.P.), the National Science Foundation (C.K. and C.A.A.), the Mathers Foundation (C.K. and C.A.A.) and the World Class University program through the National Research Foundation of Korea funded by the Ministry of Education, Science and Technology (R31-10008, C.K.).

AUTHOR CONTRIBUTIONS

C.A.A. and C.K. designed the experiments. C.A.A. and R.P. performed the experiments. C.A.A. wrote the codes and analyzed the data. C.A.A., R.P., H.M. and C.K. wrote the manuscript.

COMPETING FINANCIAL INTERESTS

The authors declare no competing financial interests.

Published online at http://www.nature.com/natureneuroscience/.
Reprints and permissions information is available online at http://www.nature.com/reprintsandpermissions/.

1. Koch, C. *Biophysics of Computation* (Oxford University Press, 1999).
2. Stuart, G., Spruston, N. & Hausser, M. *Dendrites* (Oxford University Press, 2008).
3. Haider, B. & McCormick, D.A. Rapid neocortical dynamics: cellular and network mechanisms. *Neuron* **62**, 171–189 (2009).
4. Gold, C., Henze, D.A., Koch, C. & Buzsáki, G. On the origin of the extracellular action potential waveform: a modeling study. *J. Neurophysiol.* **95**, 3113–3128 (2006).
5. Pettersen, K.H. & Einevoll, G.T. Amplitude variability and extracellular low-pass filtering of neuronal spikes. *Biophys. J.* **94**, 784–802 (2008).
6. Steriade, M., Nunez, A. & Amzica, F. A novel slow (< 1 Hz) oscillation of neocortical neurons *in vivo*: depolarizing and hyperpolarizing components. *J. Neurosci.* **13**, 3252–3265 (1993).
7. Steriade, M., Nunez, A. & Amzica, F. Intracellular analysis of relations between the slow (<1 Hz) neocortical oscillation and other sleep rhythms of the electroencephalogram. *J. Neurosci.* **13**, 3266–3283 (1993).
8. Vanderwolf, C.H. Hippocampal electrical activity and voluntary movement in the rat. *Electroencephalogr. Clin. Neurophysiol.* **26**, 407–418 (1969).
9. Buzsáki, G., Leung, L.W. & Vanderwolf, C.H. Cellular bases of hippocampal EEG in the behaving rat. *Brain Res.* **287**, 139–171 (1983).
10. Buzsáki, G. Theta oscillations in the hippocampus. *Neuron* **33**, 325–340 (2002).
11. Lubenov, E.V. & Siapas, A.G. Hippocampal theta oscillations are travelling waves. *Nature* **459**, 534–539 (2009).
12. Buzsáki, G., Horvath, Z., Urioste, R., Hetke, J. & Wise, K. High-frequency network oscillation in the hippocampus. *Science* **256**, 1025–1027 (1992).
13. Ylinen, A. *et al.* Sharp wave–associated high-frequency oscillation (200 Hz) in the intact hippocampus: network and intracellular mechanisms. *J. Neurosci.* **15**, 30–46 (1995).
14. Arvanitaki, A. Effects evoked in an axon by the activity of a contiguous one. *J. Neurophysiol.* **5**, 89–108 (1942).
15. Traub, R.D., Dudek, F.E., Taylor, C.P. & Knowles, W.D. Simulation of hippocampal afterdischarges synchronized by electrical interactions. *Neuroscience* **14**, 1033–1038 (1985).
16. Chan, C.Y. & Nicholson, C. Modulation by applied electric fields of Purkinje and stellate cell activity in the isolated turtle cerebellum. *J. Physiol. (Lond.)* **371**, 89–114 (1986).
17. Jefferys, J.G. Nonsynaptic modulation of neuronal activity in the brain: electric currents and extracellular ions. *Physiol. Rev.* **75**, 689–723 (1995).
18. Radman, T., Su, Y., An, J.H., Parra, L.C. & Bikson, M. Spike timing amplifies the effect of electric fields on neurons: implications for endogenous field effects. *J. Neurosci.* **27**, 3030–3036 (2007).
19. Deans, J.K., Powell, A.D. & Jefferys, J.G. Sensitivity of coherent oscillations in rat hippocampus to AC electric fields. *J. Physiol.* **583**, 555–565 (2007).
20. Anastassiou, C.A., Montgomery, S.M., Barahona, M., Buzsáki, G. & Koch, C. The effect of spatially inhomogeneous extracellular electric fields on neurons. *J. Neurosci.* **30**, 1925–1936 (2010).
21. Chan, C.Y., Hounsgaard, J. & Nicholson, C. Effects of electric fields on transmembrane potential and excitability of turtle cerebellar Purkinje cells *in vitro*. *J. Physiol. (Lond.)* **402**, 751–771 (1988).
22. Ozen, S. *et al.* Transcranial electric stimulation entrains cortical neuronal populations in rats. *J. Neurosci.* **30**, 11476–11485 (2010).
23. Noebels, J.L. & Prince, D.A. Development of focal seizures in cerebral cortex: role of axon terminal bursting. *J. Neurophysiol.* **41**, 1267–1281 (1978).

24. Jefferys, J.G. & Haas, H.L. Synchronized bursting of CA1 hippocampal pyramidal cells in the absence of synaptic transmission. *Nature* **300**, 448–450 (1982).
25. Ghai, R.S., Bikson, M. & Durand, D.M. Effects of applied electric fields on low-calcium epileptiform activity in the CA1 region of rat hippocampal slices. *J. Neurophysiol.* **84**, 274–280 (2000).
26. Marshall, L., Helgadottir, H., Molle, M. & Born, J. Boosting slow oscillations during sleep potentiates memory. *Nature* **444**, 610–613 (2006).
27. O'Keefe, J. & Recce, M.L. Phase relationship between hippocampal place units and the EEG theta rhythm. *Hippocampus* **3**, 317–330 (1993).
28. Fries, P., Reynolds, J.H., Rorie, A.E. & Desimone, R. Modulation of oscillatory neuronal synchronization by selective visual attention. *Science* **291**, 1560–1563 (2001).
29. Womelsdorf, T., Fries, P., Mitra, P.P. & Desimone, R. Gamma-band synchronization in visual cortex predicts speed of change detection. *Nature* **439**, 733–736 (2006).
30. Womelsdorf, T. *et al.* Modulation of neuronal interactions through neuronal synchronization. *Science* **316**, 1609–1612 (2007).
31. Colgin, L.L. *et al.* Frequency of gamma oscillations routes flow of information in the hippocampus. *Nature* **462**, 353–357 (2009).
32. Rutishauser, U., Ross, I.B., Mamelak, A.N. & Schuman, E.M. Human memory strength is predicted by theta-frequency phase-locking of single neurons. *Nature* **464**, 903–907 (2010).
33. Kamondi, A., Acsady, L., Wang, X.J. & Buzsáki, G. Theta oscillations in somata and dendrites of hippocampal pyramidal cells *in vivo*: activity-dependent phase-precession of action potentials. *Hippocampus* **8**, 244–261 (1998).
34. Weiss, S.A. & Faber, D.S. Field effects in the CNS play functional roles. *Front Neural Circuits* **4**, 15 (2010).
35. Mann, E.O. & Paulsen, O. Local field potential oscillations as a cortical soliloquy. *Neuron* **67**, 3–5 (2010).
36. Pastalkova, E., Itskov, V., Amarasingham, A. & Buzsáki, G. Internally generated cell assembly sequences in the rat hippocampus. *Science* **321**, 1322–1327 (2008).
37. Kreiman, G. *et al.* Object selectivity of local field potentials and spikes in the macaque inferior temporal cortex. *Neuron* **49**, 433–445 (2006).
38. Harvey, C.D., Collman, F., Dombeck, D.A. & Tank, D.W. Intracellular dynamics of hippocampal place cells during virtual navigation. *Nature* **461**, 941–946 (2009).
39. Kreiman, G., Koch, C. & Fried, I. Category-specific visual responses of single neurons in the human medial temporal lobe. *Nat. Neurosci.* **3**, 946–953 (2000).
40. Quiroga, R.Q., Reddy, L., Kreiman, G., Koch, C. & Fried, I. Invariant visual representation by single neurons in the human brain. *Nature* **435**, 1102–1107 (2005).
41. Logothetis, N.K., Kayser, C. & Oeltermann, A. *In vivo* measurement of cortical impedance spectrum in monkeys: implications for signal propagation. *Neuron* **55**, 809–823 (2007).
42. Montoro, R.J. & Yuste, R. Gap junctions in developing neocortex: a review. *Brain Res. Brain Res. Rev.* **47**, 216–226 (2004).
43. Histed, M.H., Bonin, V. & Reid, R.C. Direct activation of sparse, distributed populations of cortical neurons by electrical microstimulation. *Neuron* **63**, 508–522 (2009).
44. Milstein, J., Mormann, F., Fried, I. & Koch, C. Neuronal shot noise and Brownian 1/f2 behavior in the local field potential. *PLoS ONE* **4**, e4338 (2009).
45. Holt, G.R. & Koch, C. Electrical interactions via the extracellular potential near cell bodies. *J. Comput. Neurosci.* **6**, 169–184 (1999).
46. Jacobson, G.A. *et al.* Subthreshold voltage noise of rat neocortical pyramidal neurones. *J. Physiol.* **564**, 145–160 (2005).
47. Hutcheon, B. & Yarom, Y. Resonance, oscillation and the intrinsic frequency preferences of neurons. *Trends Neurosci* **23**, 216–222 (2000).
48. Kayser, C., Montemurro, M.A., Logothetis, N.K. & Panzeri, S. Spike-phase coding boosts and stabilizes information carried by spatial and temporal spike patterns. *Neuron* **61**, 597–608 (2009).
49. Tabareau, N., Slotine, J.J. & Pham, Q.C. How synchronization protects from noise. *PLOS Comput. Biol.* **6**, e1000637 (2010).

ONLINE METHODS

Slice preparation and cell identification. We quickly decapitated 14–18-d-old Wistar rats according to institutional and Swiss Federal Veterinary Office guidelines, with the authorization of the Office vétérinaire cantonal du canton de Vaud. The brain was carefully removed and placed in iced artificial cerebrospinal fluid (ACSF). We cut 300-µm-thick parasaggital slices of the primary somatosensory cortex (hind-limb area) on an HR2 vibratome (Sigmann Elektronik). Slices were incubated at 37 °C for 30–60 min and then left at 25 °C until recording. Cells were visualized by infrared differential interference contrast videomicroscopy using a VX55 camera (Till Photonics) mounted on an upright BX51WI microscope (Olympus). Thick tufted layer 5 pyramidal neurons were selected according to their large soma size (15–25 µm) and the large trunk of the apical dendrite. Care was taken to use only 'parallel' slices, that is, slices that had a cutting plane parallel to the course of the apical dendrites and the primary axonal trunk. This ensured a sufficient preservation of both the pyramidal neurons' axonal and dendritic arborizations.

Chemicals and solutions. Slices were continuously superfused with ACSF containing 125 mM NaCl, 25 mM $NaHCO_3$, 2.5 mM KCl, 1.25 mM NaH_2PO_4, 2 mM $CaCl_2$, 1 mM $MgCl_2$ and 25 mM D-glucose, bubbled with 95% O_2/5% CO_2. The intracellular pipette solution contained 110 mM potassium gluconate, 10 mM KCl, 4 mM ATP-Mg, 10 mM phosphocreatine, 0.3 mM GTP, 10 mM HEPES and 13 mM biocytin, adjusted to a pH 7.3–7.4 with 5 M KOH. Osmolarity was adjusted to 290–300 mosm with D-mannitol (25–35 mM). The membrane potential values given were not corrected for the liquid junction potential, which was approximately −14 mV. Gabazine was purchased from Tocris, CNQX disodium salt was purchased from Biotrend, and AP5 and bicuculline were purchased from Sigma-Aldrich. All experiments were performed using 20 µM gabazine or 20 µM bicuculline, 40 µM AP5 and 10 µM CNQX to avoid synaptic transmission from interfering with ephaptic signals[19].

Electrophysiological recordings. Multiple somatic whole-cell recordings (1–4 cells simultaneously) were performed with Multiclamp 700B amplifiers (Molecular Devices) in the current-clamp mode. Only recordings with seal resistance in excess of 2 GΩ were considered (mean ± s.d., 4.4 ± 1.9 GΩ). Neurons with resting potential larger than −60 mV were discarded from the analyses. The cell resistance of the patched cells was 74.9 ± 19.4 MΩ. The reference electrode in all experiments was positioned approximately 1 cm from the slice in the ACSF bath so as not to be affected by the extracellular stimulus. The temperature was 35 ± 0.5 °C during recordings. Bridge balance compensation was continuously performed during all recordings. Data acquisition was performed via an ITC-1600 board (Instrutech), connected to a personal computer running a custom-written routine in IgorPro (Wavemetrics). Sampling rates were 10 kHz and the voltage signal was filtered with a 1.2-kHz Bessel filter. Patch pipettes were pulled with a Flamming/Brown micropipette puller (DMZ Universal Puller, Zeitz-Instrumente GmbH) and had an initial resistance of 4–8 MΩ for patch recordings and 1–3 MΩ for extracellular recordings.

Intracellular stimulation was applied by MultiClamp 700B amplifiers and extracellular stimulation by a MultiClamp 700B amplifier (up to 200 nA) or via an isolated pulse stimulator (A-M Systems 2100) for higher currents in characterization experiments. Note that we tested the experimental setup (both electrodes and amplifiers) for the presence of crosstalk.

Data analysis. All data analyses were performed using custom-written MATLAB 7.9.0 programs (Mathworks).

Subthreshold analysis. To calculate the amplitude, frequency and phase of the V_i, V_e and V_m oscillations induced by the extracellular stimulus $I = I_0 \sin(2\pi ft)$, with I_0 (nA) being the amplitude and f (Hz) the frequency of the extracellular stimulus, we calculated the mean V_i, V_e and V_m waveform (as shown in **Fig. 2a**) by aligning $[0, T]$-time intervals of the raw unfiltered trace with T (s) being the period of the extracellular stimulus defined as $T = 1/f$. The duration of each experiment was 5 s. For example, to study the subthreshold behavior of the membrane when injecting an extracellular stimulus with $f = 8$ Hz, we divided the time course of the V_i, V_e and V_m traces into n_{interv} intervals of duration $T = 0.125$ s with $n_{interv} = (5\text{ s})/T = 40$. In a subsequent step, we defined the mean waveform by calculating the mean of the n_{interv} traces from 0 to T. The amplitude, frequency and phase of the mean waveform of each neuron were used for the statistical analyses shown in **Figure 2b**,**c**. The V_i trace was measured via the intracellular electrode, while the V_e trace was the one recorded by the extracellular electrode closest to the soma (typically within 15 µm).

To perform the normalized cross-correlation analyses between two signals, we first applied a fifth-order Butterworth low-pass filter to the V_i, V_e and V_m traces with a frequency limit of 100 Hz. We then used the MATLAB function xcorr to calculate the unbiased estimate of the cross-correlation function normalized by the s.d. of the two signals. The statistical comparison between the cross-correlation $\text{xcorr}(V_i, V_e)$ and $\text{xcorr}(V_m, V_e)$ was performed using the paired t test corrected with the Bonferroni-correction for multiple comparisons at $q < 0.05$.

Suprathreshold analysis. For the spike-phase calculation, the V_e trace was first bandpass-filtered using a second-order Butterworth filter with frequency limits $(f_{min}, f_{max}) = (0.2f, 2f)$ with f being the stimulation frequency of the extracellular stimulus. This way we were able to specifically study phase locking of spiking activity to the extracellular stimulus. To determine the spike phase, for example, the phase of the harmonic extracellular stimulus V_e when an action potential is elicited, we used two different methods. First, the Hilbert transform was used to calculate the instantaneous phase of the V_e closest to the soma of the spiking neuron. Second, on the basis of the mean harmonic V_e waveform, as measured at the soma by plotting all V_e waves along a single period and calculating the mean, the phase was determined by assigning every instant to the mean V_e waveform (see subthreshold analysis). The spike time was defined as the maximum of the second-order time derivative of the intracellular potential V_i right before the maximum deflection of V_i. The spike phase was then defined as the V_e phase at the spike time. The two methods of determining the V_e phase resulted in very similar outcomes but we chose to adopt the Hilbert transform as it is an instantaneous measure that determines the phase based on the instantaneous V_e fluctuation at the soma rather than assuming an average V_e waveform.

The phase was measured (in degrees) in the range [0°, 360°], where 90° is the peak and 270° the trough of the V_e waveform. To test whether a neuron was significantly phase locked, we compared the phase angles against uniformity using a Rayleigh test for statistics of circular variables. The Rayleigh test (adopted from ref. 50) was carried out at each stimulus amplitude I_0 and frequency f for all neurons ($n = 25$ cells).

The STA was calculated by extracting, for every spike, a segment of the V_e trace measured at the soma centered at the spike time. The length of the V_e segment depended on the stimulation frequency f. Because we wanted to have at least two STA cycles for each f (see **Fig. 3c**) the time window around each spike was selected ±1 s, ±0.5 s and ±0.1 s for $f = 1$, 8 and 30 Hz, respectively. We used a fifth-order lowpass Butterworth filter with frequency limits at 2, 14 and 50 Hz for the $f = 1$-, 8- and 30-Hz data, respectively, to remove the spike artifact from the STA and STP analyses (**Supplementary Figs. 4**–**9**).

The SFC is defined as the ratio between the power spectrum of the STA and the power spectrum of all power spectra of all V_e segments that were averaged to obtain the STA[28]. The latter is often referred to as the STP. The STP quantifies the oscillations that are present in the V_e signal regardless of whether they are related to the occurrence of spikes or not[28]. The STP is shown in **Supplementary Figures 4c**, **6c** and **8c**, as well as in **Supplementary Figures 5**, **7** and **9** for four individual neurons. We also found the STP of each individual neuron for the four-neuron experiment (**Fig. 4**) in **Supplementary Figures 11**–**13**. The peak of STP at f is attributed to the fact that the external stimulus has a single frequency.

We kept the number of spikes constant for each condition when comparing the SFC between different extracellular stimulations. We did this by randomly selecting a subsample of spikes from the bigger group using MATLAB's random number generator. This procedure was applied to all STAs and STPs. The difference between the SFC of control and extracellular stimulation experiments persisted regardless of the numbers of spikes used.

All statistical comparisons of differences between the SFC for different extracellular stimulation configurations (I_0, f) were corrected for multiple comparisons using the fdr procedure at $q < 0.05$. The comparisons between control and extracellular stimulation experiments for the STA spectra and SFC values for different field configurations (I_0, f) (**Fig. 3**) were performed using paired t tests.

50. Berens, P. CircStat: a MATLAB toolbox for circular statistics. *J. Stat. Softw.* **31**, 1–21 (2009).

doi:10.1038/nn.2727